



Realization of Epsilon-Near-Zero Metamaterial Stack Based on Dielectric-Semiconductor-Metal Multilayers

Mina Vafaei¹ · Mahmood Moradi¹ · Gholam Hossein Bordbar¹

Received: 9 March 2019 / Accepted: 3 June 2019 / Published online: 16 July 2019
© Springer Science+Business Media, LLC, part of Springer Nature 2019

Abstract

The epsilon-near-zero (ENZ) metamaterials are designed theoretically based on multilayer nanostructure stack with three sublayers (in each period) in the visible range for transverse magnetic mode at normal and transverse electric mode at oblique incident lights. The sublayers can be either metal, dielectric, or semiconductor materials. The effective permittivities of the multilayer metamaterial stacks are derived based on the optical nonlocality analysis that expand via the Bloch theory and transfer matrix method. Multilayer metamaterials based on dielectric-semiconductor-metal (DSM) including Al_2O_3 –Ge–Ag triple layers are considered to study their unique optical properties and determine the ENZ wavelengths at visible frequencies. Furthermore, the propagation properties of terahertz (THz) waves passing through the DSM multilayer stacks have been theoretically investigated by calculating transmission, reflection, and absorption spectra at different angles of incidence. The electric field distribution and absorption results show that the optical loss can be reduced and kept under control in multilayer metamaterial stacks. The result of reflection and transmission indicate that the DSM multilayer stacks can be introduced as a band-pass filter, and various conditions are considered for optimal filtering. In addition, it is shown that the number of depth in reflection spectra (peak in transmission spectra) increases by increasing the number of triple layers in the structures which perfectly matches with the frequencies that satisfy the Bragg's law. All analytical results are in good agreement with the results obtained from numerical simulations.

Keywords Epsilon-near-zero metamaterials · Effective permittivities · Nonlocality · Band-pass filter

Introduction

Today, design and description of nanostructured metamaterials with the purpose of realizing their optical properties that are not available in natural materials is an important and interesting field of research in various sciences [1–9]. A class of these synthetic structures that have attracted a lot of attention is epsilon-near-zero (ENZ) metamaterials where the real part of one or two components of effective permittivity becomes zero. The near-zero permittivity can be found at the infrared and optical frequencies. Some examples of these are polar dielectrics (silicon carbide), semiconductors (indium antimonide), Ag, and Au, near their plasma frequencies [2]. ENZ behavior can be realized in fabricated metamaterials. One main approach to achieve the desired

ENZ metamaterials is utilizing multilayer metal-dielectric nanostructures, which are actually attractive because of their simple fabrication. Experimental realization and theoretical investigation of an ENZ metamaterial at visible wavelength have been reported recently [3, 10, 11].

Up to now, many unique applications have been discovered for these kinds of nanostructures such as negative refraction [12, 13], subwavelength imaging [14–16], cloaking [17, 18], super absorbing [19, 20], wave guiding [21, 22], and spontaneous [23, 24] and thermal emission engineering [25, 26].

The ENZ metamaterials are introduced as angular filters [27, 28]. Alu et al. [27] showed that an ENZ planar stack allows transmission just for a particular narrow angular width, not far from the normal incidence, by acting as an angular filter for the transverse magnetic (TM) polarization. Alekseyev et al. [28] concluded that an array of silver nanowires in anodic alumina matrix can function as a narrowband angular transmittance filter and polarizer. However, to date, filtering has not been reported for multilayer (two sublayers) metamaterials. Hence, in this work, we designed a multilayer metamaterial stack which consists of three sublayers instead

✉ Mahmood Moradi
mmoradi@shirazu.ac.ir

¹ Physics Department, College of Sciences, Shiraz University, Shiraz 71946-84795, Iran

of two sublayers in conventional multilayer metamaterials. The sublayers can be either metal, dielectric, or semiconductor. The effective permittivity of multilayer metamaterials with three sublayers is derived based on the Bloch theory and transfer matrix method for the TM mode at normal and transverse electric (TE) mode at oblique incident lights. In these metamaterials, we have more control to obtain the ENZ wavelength, namely just by changing the thickness of one of the sublayers, we can have an ENZ wavelength anywhere in the visible range. Indeed in our proposed multilayer stack, one can obtain ENZ wavelength in the broader range that is not accessible in conventional multilayer stacks.

Also, the propagation properties of terahertz (THz) waves passing through the multilayer stacks have been theoretically explored via the calculated transmission, reflection, and absorption spectra at different angles of incidence. We demonstrate that the loss can be reduced and kept under control as an important issue in nanostructured metamaterials. In addition, we show that our proposed structure can act as a band-pass filter in the visible range, namely passes wavelengths within a narrow range and rejects wavelengths outside that range.

Finally, we showed that the number of depth in reflection spectra (peak in transmission spectra) is enhanced by increasing the number of periodic triple layers. Actually, there is one depth in reflection spectra (peak in transmission spectra) for each boundary between periodic triple layers. There are two, three, and four depths in the reflection spectra, for three, four, and five triple layers respectively.

It is noteworthy that all our analytical results are in good agreement with the results obtained from numerical simulations. Our numerical simulations are performed by using the finite difference time domain (FDTD) method with the software computer simulation technology (CST, Microwave Studio).

Formulas and Theoretical Analysis

Because of the subwavelength feature of the multilayer metamaterial stacks, their electromagnetic properties can be described by effective medium theory (EMT). Therefore, the effective permittivity only depends on the frequency. However, the components of permittivity depend on the frequency and wave vector due to the variation of electromagnetic field on a unit nanostructure. Then, the optical nonlocality effects with spatial dispersion occur in the multilayer stacks. Recently, the nonlocal effective parameters of metal-dielectric multilayer metamaterials have been determined based on various analyses of optical nonlocalities. These effects have been studied around the ENZ wavelength [10, 11, 29, 30].

In this study, the nonlocal effective permittivity of multilayer metamaterial stacks with three sublayers is derived based

on the Bloch theory and transfer matrix method for the TM mode at normal and TE mode at oblique incident lights.

A one-dimensional nonmagnetized periodic nanostructure is considered with three sublayers by utilizing an incident plane wave with the wave vector $\vec{k} = (k_x, 0, k_z)$ and field components (E_x, H_y, E_z) at normal incidence for the TM mode and the field components (H_x, E_y, H_z) at arbitrary angle of incidence for TE mode. The permittivity and the thickness of the three sublayers are symbolized as $\epsilon_1, d_1; \epsilon_2, d_2;$ and ϵ_3, d_3 respectively. When the geometric parameters are much smaller than the free-space wavelength (λ_0) of the incident electromagnetic wave, the underlying structure can be considered as an effective medium. Effective permittivity of the multilayer metamaterial stacks can be homogenized via Maxwell-Garnett formulas [31, 32]. For TM mode, we derived and obtained the permittivity components parallel and perpendicular to the stack layers as

$$\epsilon_{\text{eff}}^x = \epsilon_{\text{eff}}^y = f_1\epsilon_1 + f_2\epsilon_2 + f_3\epsilon_3 \tag{1}$$

$$\epsilon_{\text{eff}}^z = \frac{\epsilon_1\epsilon_2\epsilon_3}{f_1\epsilon_2\epsilon_3 + f_2\epsilon_1\epsilon_3 + f_3\epsilon_1\epsilon_2} \tag{2}$$

and for TE mode, the permittivity component can be obtained as

$$\epsilon_{\text{eff}}^y = f_1\epsilon_1 + f_2\epsilon_2 + f_3\epsilon_3 \tag{3}$$

where $f_1 = \frac{d_1}{d_1+d_2+d_3}$, $f_2 = \frac{d_2}{d_1+d_2+d_3}$, and $f_3 = \frac{d_3}{d_1+d_2+d_3}$ are the filling fraction of the three sublayers respectively. In this approach, EMT, the effective permittivity is a function of the frequency. But if we consider stack layers as a one-dimensional photonic crystal along the z direction, the dispersion relation was derived based on the Bloch theory and transfer matrix method as below

$$\begin{aligned} \cos(k_z d) = & \cos(k_1 d_1)\cos(k_2 d_2)\cos(k_3 d_3) - \gamma_{12}\sin(k_1 d_1)\sin(k_2 d_2)\cos(k_3 d_3) \\ & - \gamma_{13}\sin(k_1 d_1)\cos(k_2 d_2)\sin(k_3 d_3) - \gamma_{23}\cos(k_1 d_1)\sin(k_2 d_2)\sin(k_3 d_3) \end{aligned} \tag{4}$$

where $k^{(l)} = \sqrt{k_0^2 \epsilon_l - k_x^2}$; $l = 1, 2, 3$ and the polarization-specific parameters are given by

$$\begin{aligned} \gamma_{12}^{(\text{TM})} &= \frac{1}{2} \left(\frac{k_1 \epsilon_2}{k_2 \epsilon_1} + \frac{k_2 \epsilon_1}{k_1 \epsilon_2} \right) \gamma_{13}^{(\text{TM})} \\ &= \frac{1}{2} \left(\frac{k_1 \epsilon_3}{k_3 \epsilon_1} + \frac{k_3 \epsilon_1}{k_1 \epsilon_3} \right) \gamma_{23}^{(\text{TM})} \\ &= \frac{1}{2} \left(\frac{k_2 \epsilon_3}{k_3 \epsilon_2} + \frac{k_3 \epsilon_2}{k_2 \epsilon_3} \right) \end{aligned} \tag{5}$$

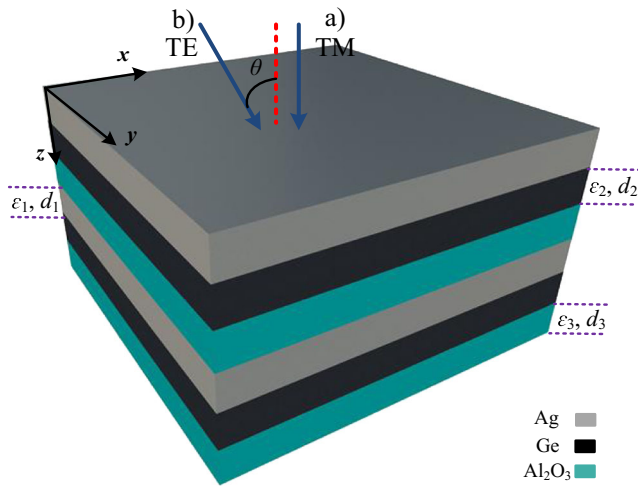


Fig. 1 Schematic illustration of multilayer metamaterial with three layers forming its period. The incident light is (a) TM mode along the z direction with the component of E_x and H_y and (b) TE mode with the components of E_y , H_x , and H_z

$$\gamma_{12}^{(TE)} = \frac{1}{2} \left(\frac{k_1}{k_2} + \frac{k_2}{k_1} \right) \quad \gamma_{13}^{(TE)} = \frac{1}{2} \left(\frac{k_1}{k_3} + \frac{k_3}{k_1} \right) \quad \gamma_{23}^{(TE)} = \frac{1}{2} \left(\frac{k_2}{k_3} + \frac{k_3}{k_2} \right) \quad (6)$$

On the other hand, if we consider the multilayer as an anisotropic stack, composed of a single material with the same total thickness, the dispersion relations of the TM and TE modes propagating in the x - z plane can be written as

$$\frac{k_z^2}{\epsilon_{\text{eff}}^x} + \frac{k_x^2}{\epsilon_{\text{eff}}^y} = k_0^2 \quad (7)$$

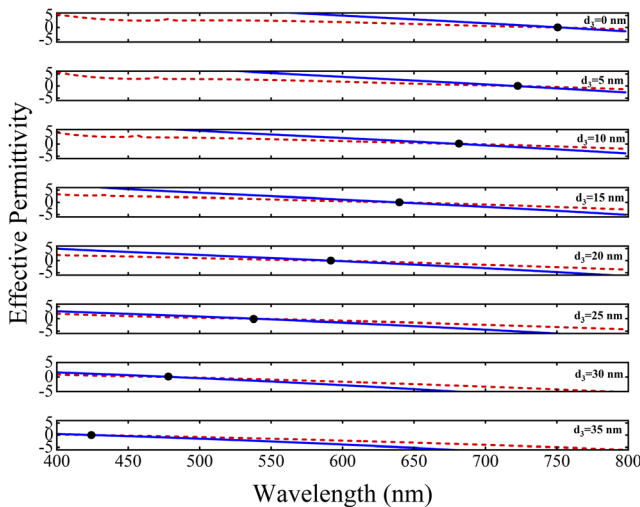


Fig. 2 The effective permittivity against the wavelength, at different thicknesses of Al_2O_3 for the total thickness of 65 nm in each period and $f_{\text{Ag}} = 0.46$. The solid points show the ENZ wavelength. The dashed red curve represents simulation and the blue solid curve represents analytical results

$$\frac{k_z^2}{\epsilon_{\text{eff}}^y} + \frac{k_x^2}{\epsilon_{\text{eff}}^x} = k_0^2 \quad (8)$$

It is worth mentioning that this conventional regime with effective permittivities given in Eqs. (7) and (8) can be obtained from Eq. (4) through the Taylor expansion up to the second order in $|k_1 d_1| \ll 1$; $|k_2 d_2| \ll 1$; $|k_3 d_3| \ll 1$; $|k_x d| \ll 1$.

Due to the Eq. (4) for TM mode at normal incidence ($k_x = 0$) and TE mode at different angles of incidence, the nonlocal effective permittivity can be derived as

$$\begin{aligned} \epsilon_{\text{eff}}^x = & \frac{1}{d^2 k_0^2} \left[\arccos^2 \left[\cos(\sqrt{\epsilon_1} k_0 d_1) \cos(\sqrt{\epsilon_2} k_0 d_2) \cos(\sqrt{\epsilon_3} k_0 d_3) \right. \right. \\ & - \frac{1}{2} \left(\sqrt{\frac{\epsilon_1}{\epsilon_3}} + \sqrt{\frac{\epsilon_3}{\epsilon_1}} \right) \sin(\sqrt{\epsilon_1} k_0 d_1) \cos(\sqrt{\epsilon_2} k_0 d_2) \sin(\sqrt{\epsilon_3} k_0 d_3) \\ & - \frac{1}{2} \left(\sqrt{\frac{\epsilon_1}{\epsilon_2}} + \sqrt{\frac{\epsilon_2}{\epsilon_1}} \right) \sin(\sqrt{\epsilon_1} k_0 d_1) \sin(\sqrt{\epsilon_2} k_0 d_2) \cos(\sqrt{\epsilon_3} k_0 d_3) \\ & \left. \left. - \frac{1}{2} \left(\sqrt{\frac{\epsilon_2}{\epsilon_3}} + \sqrt{\frac{\epsilon_3}{\epsilon_2}} \right) \cos(\sqrt{\epsilon_1} k_0 d_1) \sin(\sqrt{\epsilon_2} k_0 d_2) \sin(\sqrt{\epsilon_3} k_0 d_3) \right] \right] \end{aligned} \quad (9)$$

and

$$\begin{aligned} \epsilon_{\text{eff}}^y = & \frac{1}{d^2 k_0^2} \left[\arccos^2 \left[\cos(k_1 d_1) \cos(k_2 d_2) \cos(k_3 d_3) \right. \right. \\ & - \frac{1}{2} \left(\frac{k_1}{k_3} + \frac{k_3}{k_1} \right) \sin(k_1 d_1) \cos(k_2 d_2) \sin(k_3 d_3) \\ & - \frac{1}{2} \left(\frac{k_1}{k_2} + \frac{k_2}{k_1} \right) \sin(k_1 d_1) \sin(k_2 d_2) \cos(k_3 d_3) \\ & - \frac{1}{2} \left(\frac{k_3}{k_2} + \frac{k_2}{k_3} \right) \cos(k_1 d_1) \sin(k_2 d_2) \sin(k_3 d_3) \\ & \left. + \sin^2(\theta) \right] \end{aligned} \quad (10)$$

respectively. As illustrated in Fig. 1(b), θ is the angle of incidence in free space and $k_x = k_0 \sin(\theta)$. To confirm the results,

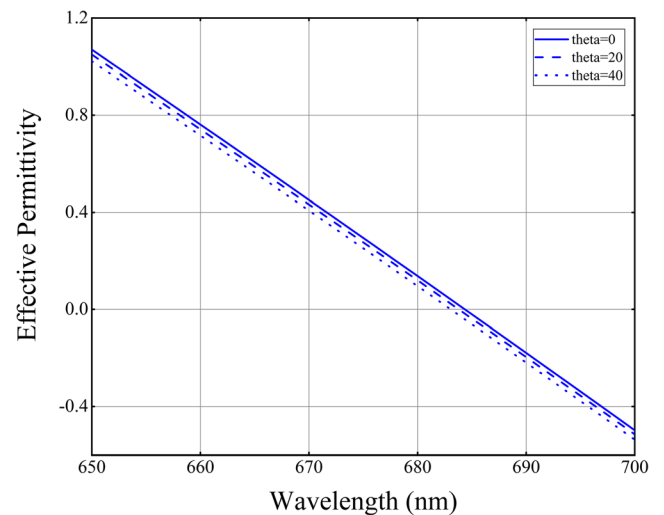
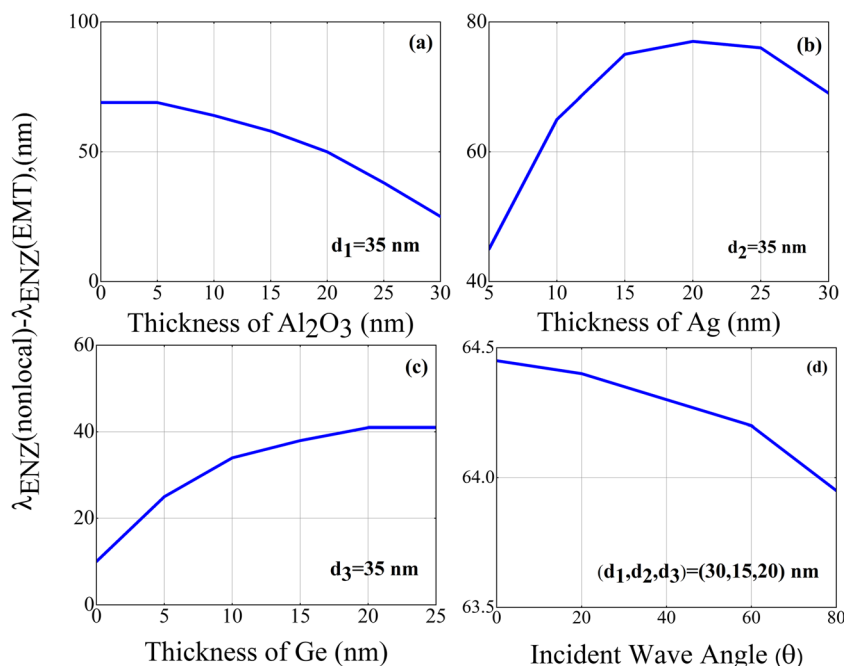


Fig. 3 The effective permittivity against the wavelength, at different angles of incidence for $\text{Al}_2\text{O}_3(10\text{nm}) - \text{Ge}(25\text{nm}) - \text{Ag}(30\text{nm})$ stack

Fig. 4 The ENZ wavelength difference versus the thickness of (a) Al₂O₃, (b) Ag, (c) Ge, and (d) angle of incidence



the effective permittivity of the multilayer metamaterials with two sublayers is obtained by setting one of the three sublayers' thicknesses to zero.

In the following, one type of ENZ metamaterial stacks, dielectric-semiconductor-metal (DSM), is introduced to study their unique optical properties and locate the ENZ wavelengths at visible frequencies.

Dielectric-Semiconductor-Metal Multilayer Metamaterials

Here multilayer metamaterial stacks based on dielectric-semiconductor-metal (DSM) including Al₂O₃ – Ge – Ag triples are considered and introduced to study their unique optical properties and obtain the ENZ wavelengths at visible frequencies. Figure 1 shows the schematic diagram of these kinds of nanostructures with two multilayers as we used in our calculations. The DSM multilayer stacks composed of Al₂O₃, Ge, and Ag are considered for the TE mode of incident light with $f_{\text{Ag}} = 0.46$ (filling fraction of Ag) and total thickness of 65 nm in each period. The permittivities of Al₂O₃, Ge, and Ag are assumed to be $\epsilon_{\text{Al}_2\text{O}_3} = 3.12$, $\epsilon_{\text{Ge}} = 16.2$, and $\epsilon_{\text{Ag}} = \epsilon_\infty - \frac{\omega_p^2}{\omega(\omega + i\gamma_c)}$ (Drude model), for the entire frequency region of our interest. For Ag, the high-frequency permittivity, the bulk plasma frequency, and the collision frequency are $\epsilon_\infty = 5$, $\omega_p = 13.4 \times 10^{15}$ rad/s, and $\gamma = 0.14 \times 10^{15}$ rad/s respectively. The thickness of the sublayers are labeled as $d_{\text{Ag}} = d_1$, $d_{\text{Ge}} = d_2$, and $d_{\text{Al}_2\text{O}_3} = d_3$. For the given constant filling fraction of Ag, the effective permittivity with respect to wavelength, at different thicknesses of Al₂O₃, is plotted in Fig. 2. The ENZ wavelengths of Al₂O₃ – Ge – Ag are shown by solid points where these wavelengths vary from 420 to 750 nm. While according to this figure, by considering the semiconductor-metal ($d_3 = 0$) multilayer of Ge – Ag or dielectric-metal ($d_2 = 0$) multilayer of Al₂O₃ – Ag with the same conditions (the total thickness of 65 nm in each period and $f_{\text{Ag}} = 0.46$), the ENZ occurs at only one wavelength for

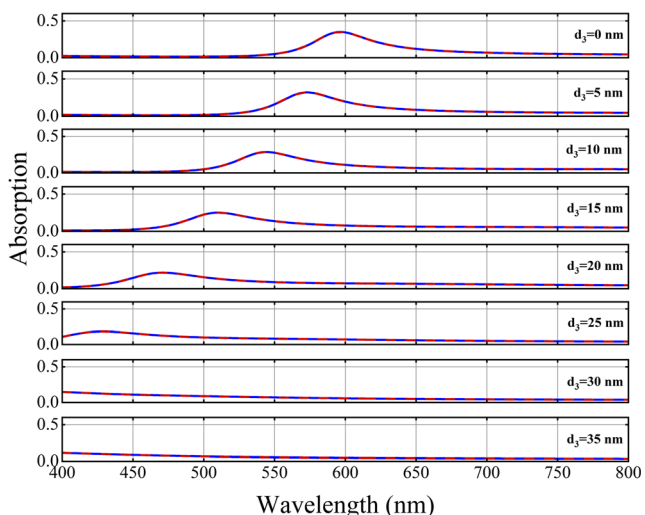
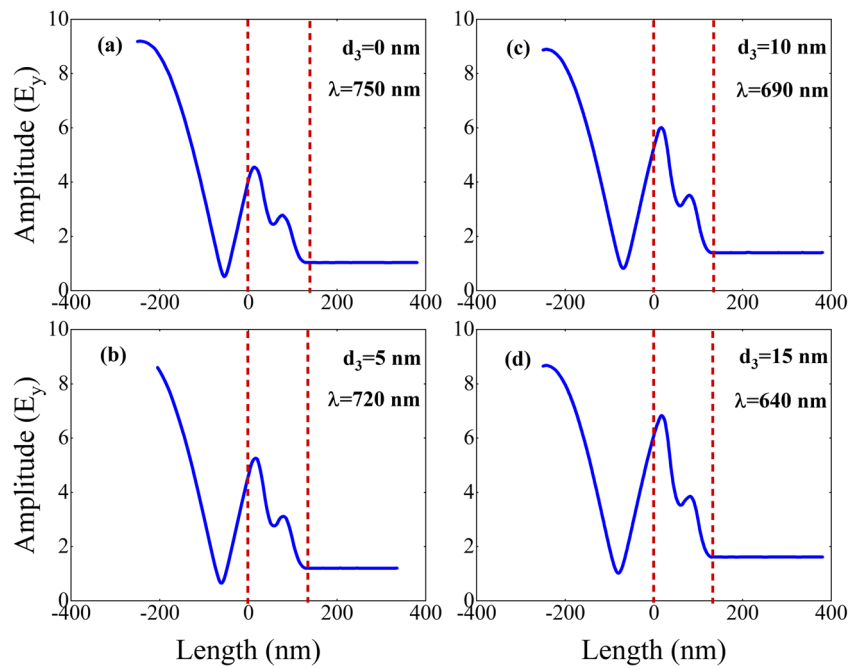


Fig. 5 The reduction trend of absorption of Ge – Ag multilayer by adding Al₂O₃ as a third layer with different thicknesses while the total thickness and f_{Ag} are constant. The dashed red curve represents simulation and blue curve represents analytical results

Fig. 6 The electric field distribution along the propagation direction for DSM multilayer at the ENZ wavelength of (a) 750 nm, (b) 720 nm, (c) 690 nm, and (d) 640 nm. By increasing the thickness of the d_3 layer, the electric field amplitude is increased due to the reduction of optical loss



each case. Therefore, in our multilayer metamaterials, we have more control to obtain the ENZ wavelength. In fact, an ENZ wavelength can be obtained anywhere in the visible range just by changing the thickness of one of the sublayers. Indeed, in our proposed multilayer stack, one can obtain ENZ wavelength in the broader range that is not accessible in conventional multilayer stacks.

According to Eq. (10), the effective permittivity of $\text{Al}_2\text{O}_3(10\text{nm}) - \text{Ge}(25\text{nm}) - \text{Ag}(30\text{nm})$ stack at different angles are plotted in Fig. 3. It is shown that the non-local ENZ wavelength of the DSM multilayer depends on the angle of incident light for the TE mode. Also, by increasing the angle of incidence, the ENZ wavelength goes down to shorter wavelengths. The ENZ wavelength difference, $\Delta\lambda_{\text{ENZ}}$, due to optical nonlocality can be calculated as

$$\Delta\lambda_{\text{ENZ}} = \lambda_{\text{ENZ}}^{\text{nonlocal}} - \lambda_{\text{ENZ}}^{\text{EMT}} \quad (11)$$

To clarify the optical nonlocality in the multilayer stacks, the variation of ENZ wavelength difference with respect to the thickness of sublayers and angle of incidence is plotted in Fig. 4. In these plots, the total thickness is assumed to be constant. It is clear that the difference of ENZ wavelength and thereby the optical nonlocality increase by increasing the thickness of the silver and germanium sublayers and decrease by increasing the thickness of Al_2O_3 (Fig. 4(a)–(c)). In Fig. 4(d), the dependency of $\Delta\lambda_{\text{ENZ}}$ on the angle of incidence is presented for TE mode. It is shown that $\Delta\lambda_{\text{ENZ}}$ decreases by

increasing the incident angle; therefore, the optical nonlocality is maximum for normal incidence.

Reduced loss is another advantage in these multilayer metamaterials. Actually, by choosing the appropriate third sublayer, loss can be reduced and are kept under control in proposed nanostructures. In Fig. 5, the absorption of the multilayer stack with respect to wavelength for different thicknesses of Al_2O_3 is illustrated while the total thickness and f_{Ag} are constant. In this case, by adding Al_2O_3 layer to the Ge – Ag multilayer as the third layer, the absorption and consequently the loss are reduced in the visible range.

As we know, the amplitude of electric field in the multilayer metamaterials decays due to the optical loss. So the electric field amplitude becomes too low after crossing the stack [10]. To confirm the reduction of loss in our three-layer stack, we have calculated the electric field distribution along the propagation direction at the ENZ wavelength via simulation method. The results showed that in DSM multilayer stack, the amplitude of electric field relatively increases by increasing the d_3 layer which means the electric field decreases slowly (Fig. 6).

Filtering by Dielectric-Semiconductor-Metal Multilayer Metamaterials

In this section, it is shown that the dielectric-semiconductor-metal multilayers can be introduced as a band-pass filter in the visible range and various conditions are examined for suitable

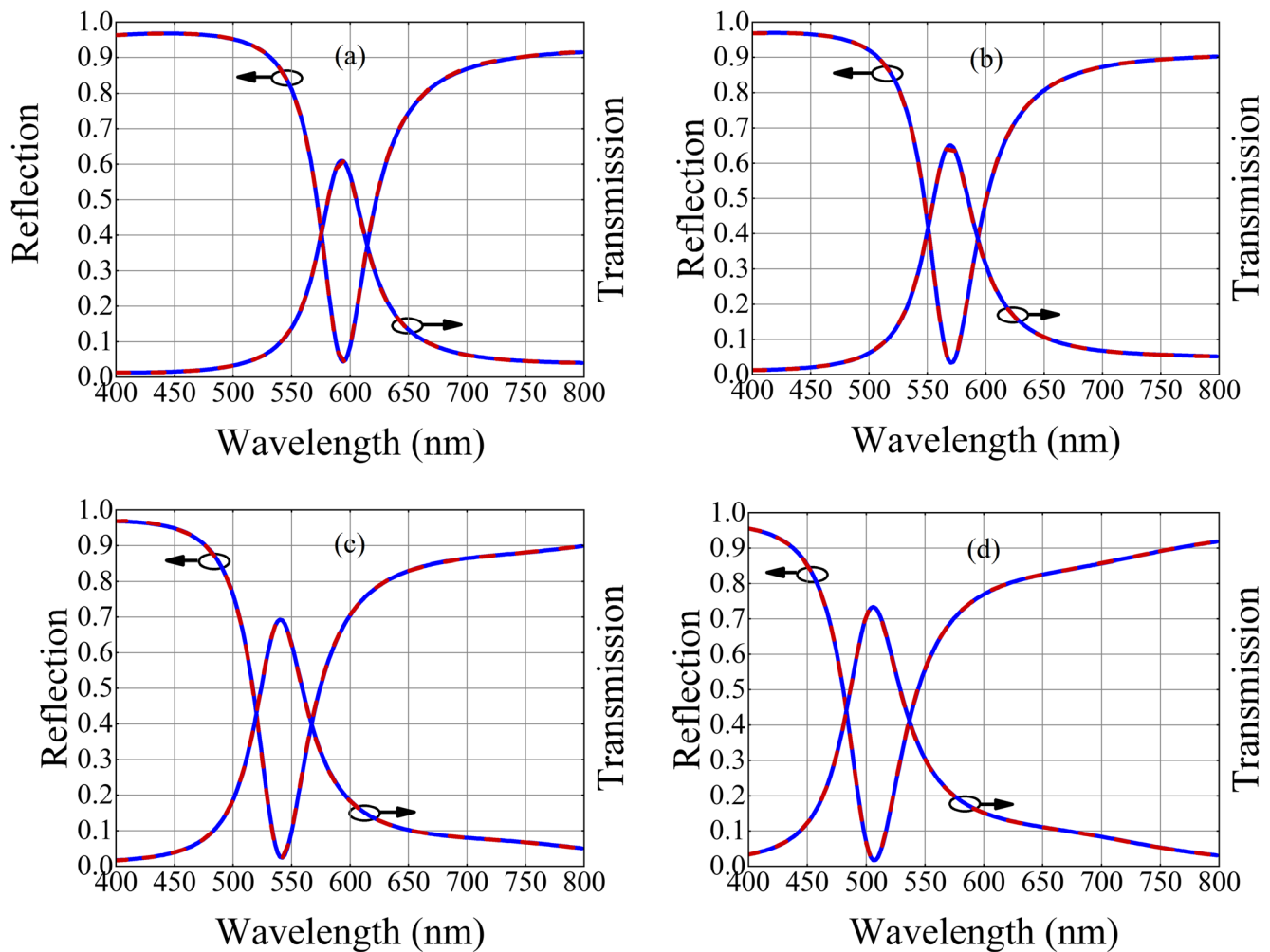


Fig. 7 The transmission and reflection spectra of Al_2O_3 –Ge–Ag for (a) $d_3 = 0$ nm, (b) $d_3 = 5$ nm, (c) $d_3 = 10$ nm, and (d) $d_3 = 15$ nm. The dashed curves represent simulation and solid curves represent analytical results

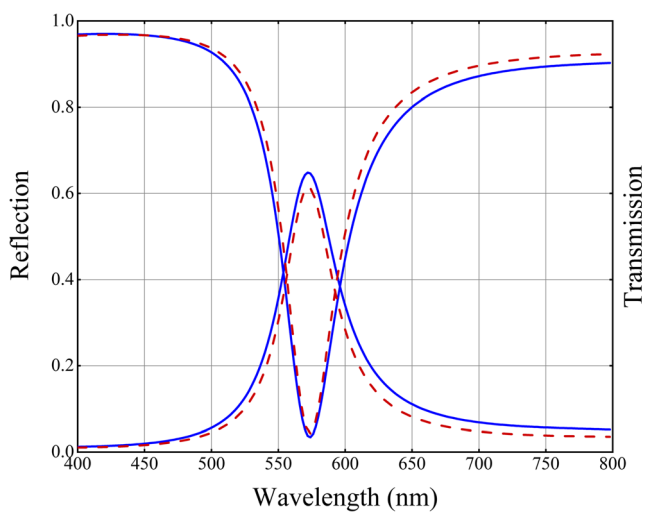


Fig. 8 The effect of the third layer in each period on filtering. The dashed curve represents transmission and reflection of Ge– Al_2O_3 –Ag multilayer stack. The solid curve represents transmission and reflection of Al_2O_3 –Ge–Ag multilayer stack

filtering. Figure 7(a)–(d) illustrates transmission and reflection spectra of Al_2O_3 –Ge–Ag stack for different thicknesses of Al_2O_3 and Ge where the total thickness of the stack and silver thickness are assumed to be the same. As the figure shows, the reflection spectra have a relatively narrow depth (transmission spectra have a peak) in the visible range. Also, as the thickness of Al_2O_3 layer is increasing, the depth in reflection (peak in transmission spectra) becomes deeper (higher) and wider. These effects are happening because by increasing the thickness of the Al_2O_3 layer, the thickness of the Ge layer reduces and since the refractive index of Al_2O_3 is less than that of Ge, the optical path is reduced in the total thickness; therefore, the electric field decays less. In addition, with the same reason and according to Bragg's law, the position of the depth in reflection (peak in transmission spectra) decreases and takes place at shorter wavelengths.

The effect of the type of third layer in each period on filtering is calculated and plotted in Fig. 8. It should be mentioned that the filtering is only achieved if the third layer in each period should be either Al_2O_3 or Ge. As Fig. 8 shows, if

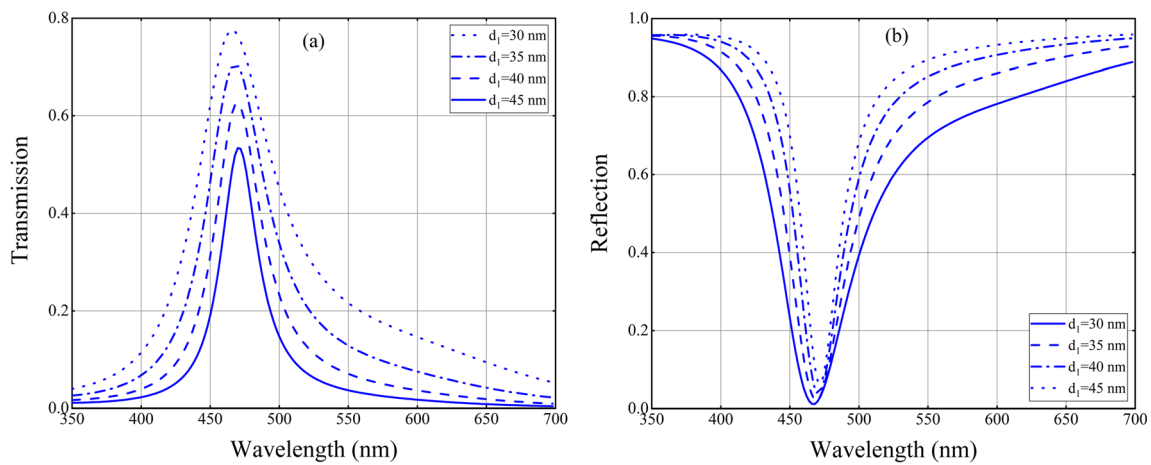


Fig. 9 (a) The transmission and (b) reflection versus wavelength of incident light at different Ag thicknesses

the third layer is Ge, the band width of filtering is narrower and the suitable filter will be obtained.

In Fig. 9, the effect of the thickness enhancement of the metal layer on filtering is investigated. As shown in this figure, if the thickness of the silver layer increases in each period, a thinner with smaller height for transition is obtained; therefore, the loss in the system is relatively high. In the reflection spectra, a similar behavior occurred but with less variation in the depths. According to the results obtained in this section and the trend of the thickness variations of sublayers, optimal filtering conditions can be achieved from dielectric-semiconductor-metal multilayers.

Another essential point in the dielectric-semiconductor-metal multilayers is the number of triple layers in the structure. As it is mentioned before, our results are obtained for two triple layers. Here we have calculated the transmission and reflection for more than two triple layers. Figure 10 shows the reflection spectra of the stack containing three, four, and five triple layers. As can be seen, there is one depth in reflection spectra (peak in transmission spectra) for each boundary between periodic triple layers. For example, there are two, three, and four depths in the reflection spectra for three, four, and five triple layers respectively. It should be noted that the transmission and reflection spectra are obtained for TM and

TE mode at normal incidence. According to our calculations, this trend is also observed for both modes at oblique incidence; however, by increasing the incident angle, the depths in the reflection spectra (peaks in transmission spectra) take place at shorter wavelengths.

These depths in the reflection spectra (peaks in transmission spectra) are related to the Bragg’s law. To make it clear, the normalized real part of the band structure, together with the transmission and reflection spectra of the multilayer stack, with respect to the normalized frequency, is plotted in Fig. 11. The normalized wave vector k_z/k_p and normalized frequency ω/ω_p are used in the band structure. Where k_z is obtained from Eq. (4), the plasma frequency of Ag is $\omega_p = 13.4 \times 10^{15}$ rad/s and plasma wave vector is defined as $k_p = \omega_p/c$. As shown in these figures, the peaks of the transmission spectra (depths in the reflection spectra) are quite consistent with the zigzag points in the band structure diagram that satisfy the Bragg’s law.

Conclusion

In summary, we designed a new epsilon-near-zero metamaterial theoretically based on multilayer metamaterial

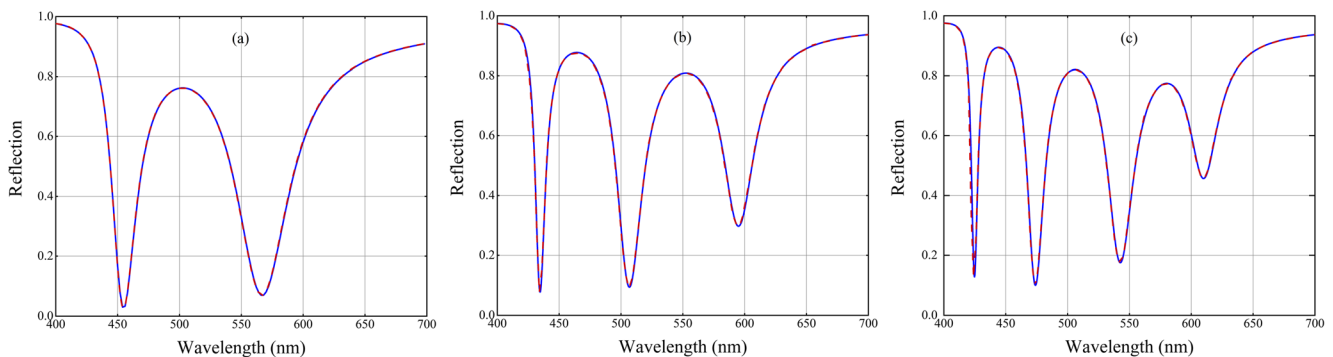


Fig. 10 The effect of periodic triple layer number in reflection spectra. The reflection spectra of $Al_2O_3 - Ge - Ag$ for (a) 3, (b) 4, and (c) 5 triple layers. The dashed red curve represents simulation results and solid blue curve represents analytical results

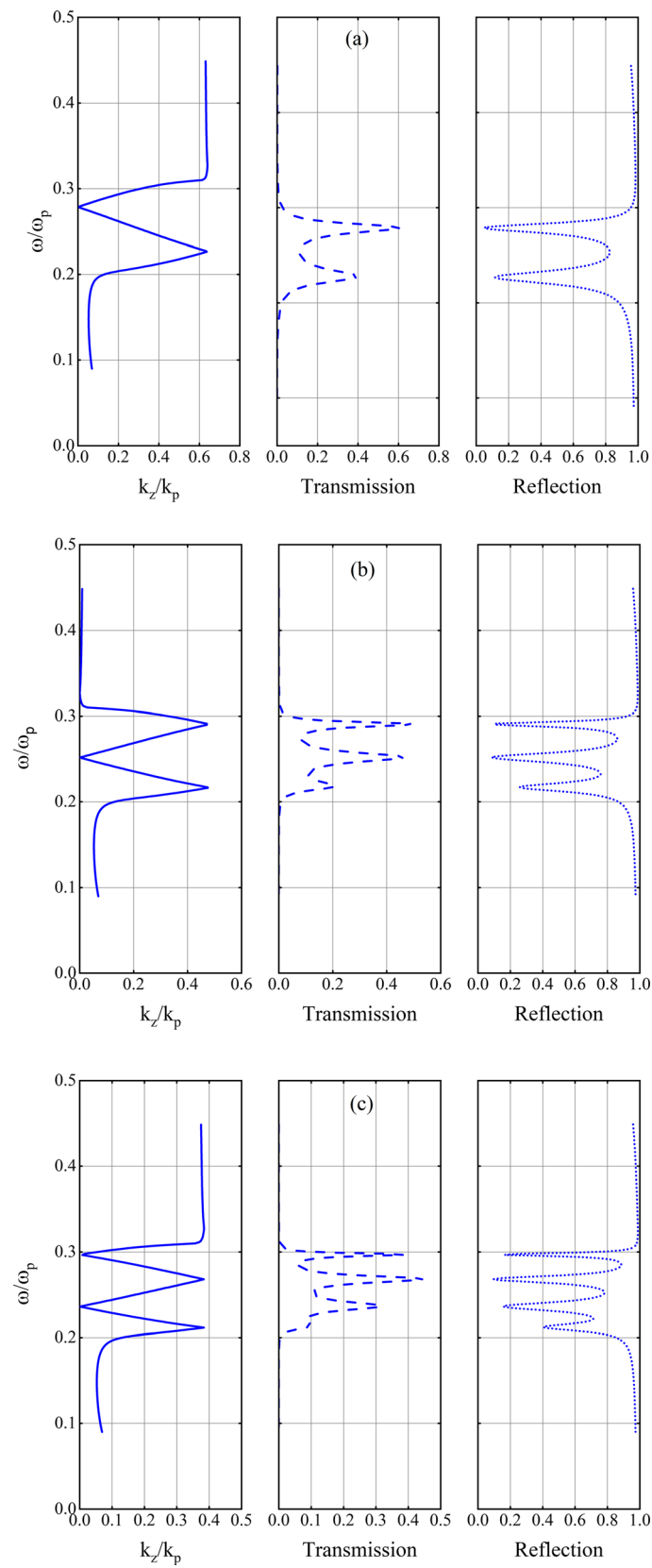


Fig. 11 The real part of the band structure together with the transmission and reflection of Al_2O_3 –Ge–Ag for (a) 3, (b) 4, and (c) 5 triple layers

stacks which consist of three sublayers instead of two sublayers in conventional multilayer metamaterials. We derived the effective permittivity of multilayer metamaterials based on the Bloch theory and transfer matrix method for TM mode at normal and TE mode at oblique incident lights. It is shown that one can obtain ENZ wavelength in the broader range by changing the thickness of one of the sublayers that is not accessible in conventional multilayer stack. The results of variation of ENZ wavelength show that the optical nonlocality in the multilayer metamaterial stacks decreases with increasing thickness of Al_2O_3 and incident angle. The propagation properties of terahertz (THz) waves passing through the multilayer stack show that DSM multilayer metamaterials can be introduced as a band-pass filter and these results are dependent on the number of periodic triple layers which is in full agreement with Bragg's law.

References

- Cai W, Shalaev V, Paul DK (2010) Optical metamaterials: fundamentals and applications. Springer, New York
- Silveirinha MG, Al'u A, Edwards B, Engheta N (2008) Overview of theory and applications of epsilon-near-zero materials. URSI General Assembly, Chicago, IL
- Maas R, Parsons J, Engheta N, Polman A (2013) Experimental realization of an epsilon-near-zero metamaterial at visible wavelengths. *Nat Photonics* 7:907–912
- Du Y, Wei W, Zhang X, Li Y (2018) Tuning metamaterials nanostructure of Janus gold nanoparticle film for surface-enhanced Raman scattering. *J Phys Chem C* 122(14):7997–8002
- Tumkur T, Barnakov Y, Kee ST, Noginov MA, Liberman V (2015) Permittivity evaluation of multilayered hyperbolic metamaterials: ellipsometry vs. reflectometry. *Appl Phys* 117:103104
- Menon L, Lu WT, Friedman AL, Bennett SP, Heiman D, Sridhar S (2008) Negative index metamaterials based on metal-dielectric nanocomposites for imaging applications. *Appl Phys Lett* 93:123117
- Sun L, Yang XD, Wang W, Gao J (2015) Diffraction-free optical beam propagation with near-zero phase variation in extremely anisotropic metamaterials. *Opt* 17(3):035101
- Sun L, Gao J, Yang X (2016) Optical nonlocality induced Zitterbewegung near the Dirac point in metal-dielectric multilayer metamaterials. *Opt Express* 24:7055–7062
- Zhang X, Zhao Z, Liu L, Li Y (2019) Design of gold nanorods Janus membrane for efficient and high-sensitive surface-enhanced Raman scattering and tunable surface plasmon resonance. *Chem Phys Lett* 721:117–122
- Gao J, Sun L, Deng H, Mathai CJ, Gangopadhyay S, Yang X (2013) Experimental realization of epsilon near-zero metamaterial slabs with metal-dielectric multilayers. *Appl Phys Lett* 103(5):051111
- Sun L, Cheng F, Mathai CJ, Gangopadhyay S, Gao J, Yang X (2014) Experimental characterization of optical nonlocality in metal-dielectric multilayer metamaterials. *Opt Express* 22:22974–22980
- Chui ST, Chan CT, Lin ZF (2006) Multilayer structures as negative refractive and lefthanded materials. *Phys: Condens Matter* 18:L89–L95
- Zhao J, Gao J, Deng Y, Liu H, Wang X (2014) Negative refraction by a planar Ag SiO₂ multilayer at ultraviolet wavelength to the limit of silver. *AIP Adv* 4:047127
- Pendry JB (2000) Negative refraction makes a perfect lens. *Phys Rev Lett* 85(18):3966–3969
- Milton GW, Nicorovici NAP, McPhedran RC, Podolskiy VA (2005) A proof of superlensing in the quasistatic regime, and limitations of superlenses in this regime due to anomalous localized resonance. *Proc R Soc Math Phys Eng Sci* 461(2064):3999–4034
- Jacob Z, Alekseyev LV, Narimanov E (2006) Optical hyperlens: far-field imaging beyond the diffraction limit. *Opt Express* 14(18):8247–8256
- Schurig D, Mock JJ, Justice BJ, Cummer SA, Pendry JB, Starr AF, Smith DR (2006) Metamaterial electromagnetic cloak at microwave frequencies. *Science* 314(5801):977–980
- Milton GW, Nicorovici NAP (2006) On the cloaking effects associated with anomalous localized resonance. *Proc R Soc Math Phys Eng Sci* 462(2074):3027–3059
- Guclu C, Campione S, Capolino F (2012) Hyperbolic metamaterial as super absorber for scattered fields generated at its surface. *Phys Rev B* 86(20):205130
- Sreekanth KV, Elkabbash M, Alapan Y, Rashed AR, Gurkan UA, Strangi G (2016) A multiband perfect absorber based on hyperbolic metamaterials. *Sci Rep* 6:26272
- Erfannia H, Rostami A (2013) Group velocity reduction in multilayer metamaterial waveguide. *Optik-Int J Light Electron Optics* 124(12):1230–1233
- He Y, He S, Gao J, Yang X (2012) Nanoscale metamaterial optical waveguides with ultrahigh refractive indices. *Optical Soc Am B* 29(9):2559–2566
- Jacob Z, Smolyaninov II, Narimanov EE (2012) Broadband Purcell effect: radiative decay engineering with metamaterials. *Appl Phys Lett* 100(18):181105–181104
- Iorsh I, Poddubny A, Orlov A, Belov P, Kivshar YS (2011) Spontaneous emission enhancement in metal-dielectric metamaterials. *Phys Lett A* 376(3):185–187
- Guo Y, Cortes CL, Molesky S, Jacob Z (2012) Broadband super-Planckian thermal emission from hyperbolic metamaterials. *Appl Phys Lett* 101(13):131106–131105
- Biehs SA, Tschikin M, Ben-Abdallah P (2012) Hyperbolic metamaterials as an analog of a blackbody in the near field. *Phys Rev Lett* 109(10):104301
- Alu A, Silveirinha MG, Salandrino A, Engheta N (2007) Epsilon-near-zero metamaterials and electromagnetic sources: tailoring the radiation phase pattern. *Phys Rev B* 75:155410
- Alekseyev LV, Narimanov EE, Tumkur T, Li H, Barnakov YA, Noginov MA (2010) Uniaxial epsilon-near-zero metamaterial for angular filtering and polarization control. *Appl Phys Lett* 97:131107
- Sun L, Li Z, Luk TS, Yang X, Gao J (2015) Nonlocal effective medium analysis in symmetric metal-dielectric multilayer metamaterials. *Phys Rev B* 91(19):195147
- Sun L, Yang X, Gao J (2016) Analysis of nonlocal effective permittivity and permeability in symmetric metal-dielectric multilayer metamaterials. *Opt* 18:065101
- Sihvola A (1999) Electromagnetic mixing formulas and applications. *IEE Electromagnetic Waves Series* 47
- Foss CA, Hornyak GL, Stockert JA, Martin CR (1994) Template synthesized nanoscopic gold particles: optical spectra and the effects of particle size and shape. *Phys Chem* 98:2963–2971

Publisher's Note Springer Nature remains neutral with regard to jurisdictional claims in published maps and institutional affiliations.